

Beyond Node Attention: Multi-Scale Harmonic Encoding for Feature-Wise Graph Message Passing

Longlong Li^{a,b}, Cunquan Qu^{b,*}, Guanghui Wang^a

^a*School of Mathematics, Shandong University, Jinan, 250100, China*

^b*Data Science Institute, Shandong University, Jinan, 250100, China*

Abstract

Conventional Graph Neural Networks (GNNs) aggregate neighbor embeddings as holistic vectors, lacking the ability to identify fine-grained, direction-specific feature relevance. We propose **MSH-GNN** (Multi-Scale Harmonic Graph Neural Network), a novel architecture that performs feature-wise adaptive message passing through node-specific harmonic projections. For each node, MSH-GNN dynamically projects neighbor features onto frequency-sensitive directions determined by the target node’s own representation. These projections are further modulated using learnable sinusoidal encodings at multiple frequencies, enabling the model to capture both smooth and oscillatory structural patterns across scales. A frequency-aware attention pooling mechanism is introduced to emphasize spectrally and structurally salient nodes during readout. Theoretically, we prove that MSH-GNN approximates shift-invariant kernels and matches the expressive power of the 1-Weisfeiler–Lehman (1-WL) test. Empirically, MSH-GNN consistently outperforms state-of-the-art models on a wide range of graph and node classification tasks. Furthermore, in challenging classification settings involving joint variations in graph topology and spectral frequency, MSH-GNN excels at capturing structural asymmetries and high-frequency modulations, enabling more accurate graph discrimination.

Keywords: Graph Neural Networks, Message Passing, Harmonic Encoding, Frequency Modulation, Node-Specific Projection, Attention Pooling

1. Introduction

Graph Neural Networks (GNNs) [1, 2, 3] have become powerful tools for learning on graph-structured data, achieving strong performance in a wide range of domains, including molecular property prediction [4], protein classification [5], and social network analysis [6]. At the core of most GNNs lies a message passing mechanism, where each node updates its representation by aggregating features from its neighbors [7].

However, conventional GNNs typically treat neighbor embeddings as holistic vectors, applying shared transformations across all feature dimensions. This coarse-grained design fails to distinguish which specific directions within the feature space are truly relevant to the target node. For instance, in molecular graphs, different feature dimensions may encode spatial, chemical, or functional signals, whose importance depends heavily on the local structural context.

Recent attention-based GNNs (e.g., GAT [8], GATv2 [9], GAAN [10], DropEdge [11], Graphormer [12], GTrans [13]) introduce node-level adaptivity by assigning scalar attention weights to neighbors. However, these models still operate on full-node embeddings, implicitly assuming uniform importance across all feature dimensions once a node is selected. This strong assumption limits their expressiveness and hinders fine-grained information flow.

While more recent models—such as GNN-FiLM [14], GraphGPS [15], and SpecFormer [16]—have explored channel-wise modulation or global spectral encodings, they lack mechanisms for localized, direction-sensitive message construction. In contrast, we propose a feature-wise message passing framework where each node projects incoming neighbor features onto task-relevant directions conditioned on its own representation. These projections are further modulated through multi-scale sinusoidal encoding, enabling frequency-aware message aggregation that bridges attention-based and spectral approaches.

This limitation is illustrated in Figure 1, where two star graphs G_1 and G_2 have neighbors with similar average features but differ in directional arrangement. GAT assigns scalar attention weights to entire neighbor embeddings and aggregates them as-is, making it insensitive to directional permutation. In contrast, our model projects each neighbor’s features into node-specific, frequency-sensitive directions, allowing it to detect such structural discrepancies.

To address these limitations, we propose **MSH-GNN** (Multi-Scale Harmonic Graph Neural Network), a novel architecture (Figure 2) that performs *feature-wise adaptive message passing* through three core stages: First, for each edge ($u \rightarrow v$), the target node v generates node-adaptive frequency bases and phase shifts to project u ’s features into *direction-sensitive subspaces* (Figure 2a). These projections are then modulated via *multi-scale sinusoidal functions* at fixed harmonic frequencies, encoding local variations and global regularities in the graph

*Corresponding author

Email addresses: longlee@mail.sdu.edu.cn (Longlong Li),
cqqu@sdu.edu.cn (Cunquan Qu), ghwang@sdu.edu.cn (Guanghui Wang)

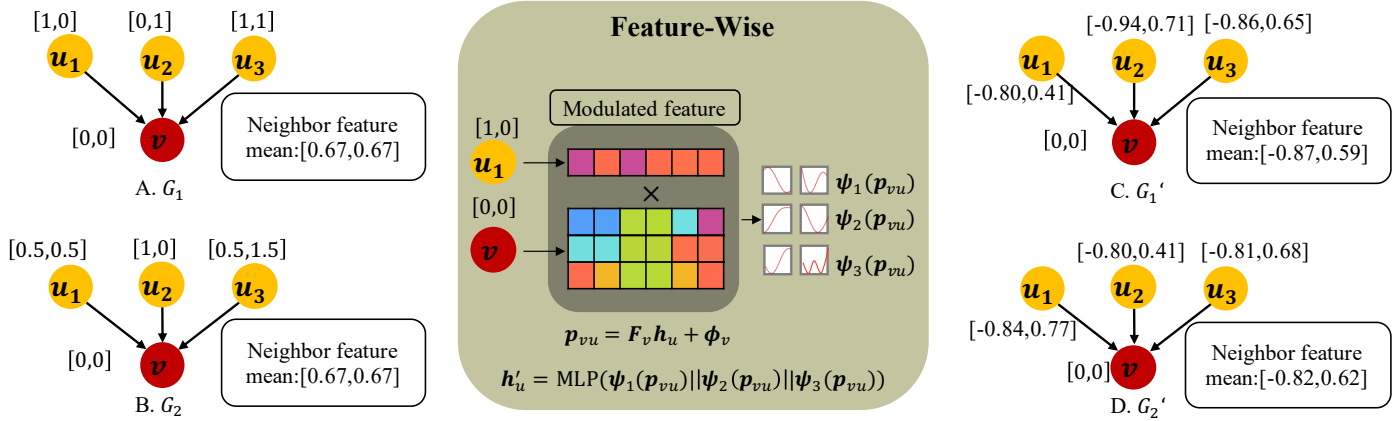


Figure 1: **MSH-GNN vs GAT.** (A) and (B): Two graphs G_1 and G_2 have identical center node features and the same neighbor feature mean $[0.67, 0.67]$, making them indistinguishable to GAT, which applies scalar attentions and aggregates full vectors uniformly. (C) and (D): MSH-GNN encodes directional composition via node-specific projections and multi-frequency sinusoidal modulation. Each edge message $h'_{vu} = \text{MLP}(\psi_1(p_{vu}) || \psi_2(p_{vu}) || \psi_3(p_{vu}))$ captures fine-grained directional asymmetry, enabling distinction between G_1 and G_2 . See Appendix Appendix B for formal details.

structure (Figure 2b). The resulting frequency-aware messages guide neighbor aggregation. Next, MSH-GNN performs *frequency-aware attentional pooling* across nodes, where modulation responses determine the contribution of each node to the graph-level embedding (Figure 2c). Finally, a multilayer perceptron classifier processes the pooled representation for downstream prediction (Figure 2d). This directional and frequency-aware pipeline allows MSH-GNN to adaptively extract salient features across multiple structural scales, bridging spectral and spatial inductive biases.

Our contributions are summarized as follows:

- We propose a feature-wise adaptive message passing scheme based on node-specific harmonic projections, enabling direction-sensitive feature selection during neighbor aggregation.
- We introduce a multi-scale harmonic modulation mechanism with learnable sinusoidal encodings to capture both global and localized structural patterns.
- We design a frequency-aware attention pooling method to highlight spectrally informative nodes in graph-level representations.
- Extensive experiments on molecular, protein, and social benchmarks demonstrate that MSH-GNN achieves state-of-the-art performance and superior structure–frequency discrimination ability.

2. Related Work

2.1. Message Passing and Feature Modulation in GNNs

Message passing lies at the core of most GNN architectures. Early models such as GCN [1], GraphSAGE [2], and GIN [3] follow a uniform paradigm where neighbor embeddings are aggregated and transformed in a holistic manner. However, this design lacks mechanisms to identify task-relevant directions in

feature space, limiting the capacity to model directional asymmetries or frequency-sensitive variations in local structures.

To improve adaptivity, feature-wise modulation has been explored. GNN-FiLM [14] applies static, channel-wise affine transformations to node features, introducing limited adaptivity but remaining node-invariant and detached from local structural context. SpecFormer [16] introduces global spectral tokens derived from Laplacian eigenvectors to guide downstream prediction, but its modulation is applied only during readout, lacking integration into node-wise message construction.

Directional and anisotropic propagation mechanisms have also been studied. Directional GNNs [17] incorporate geometric derivatives to encode anisotropy, but their directional basis is pre-defined and does not adapt to node-specific contexts. SpecFormer [16] employs sinusoidal embeddings over fixed eigenvectors to encode spectral priors, but this approach remains token-invariant and does not capture edge-level or target-conditioned modulation.

In contrast, our MSH-GNN performs *node-conditioned harmonic projections* on each neighbor, producing *localized, direction-sensitive* embeddings that adapt to both spectral and structural context of the target node.

2.2. Attention Mechanisms and Token-Based Models

To improve expressiveness over uniform message passing, attention-based GNNs such as GAT [8], GATv2 [9], and Graphormer [12] compute attention scores to assign different weights to neighbors. While effective in capturing node-level importance, these models still aggregate entire embeddings uniformly, without resolving directional relevance among feature dimensions.

Token-based transformer variants, including TokenGT [18] and GraphGPS [15], treat nodes or anchor points as tokens and apply global attention across graph elements. These methods model long-range dependencies but typically lack spatial-frequency sensitivity and fail to perform localized message

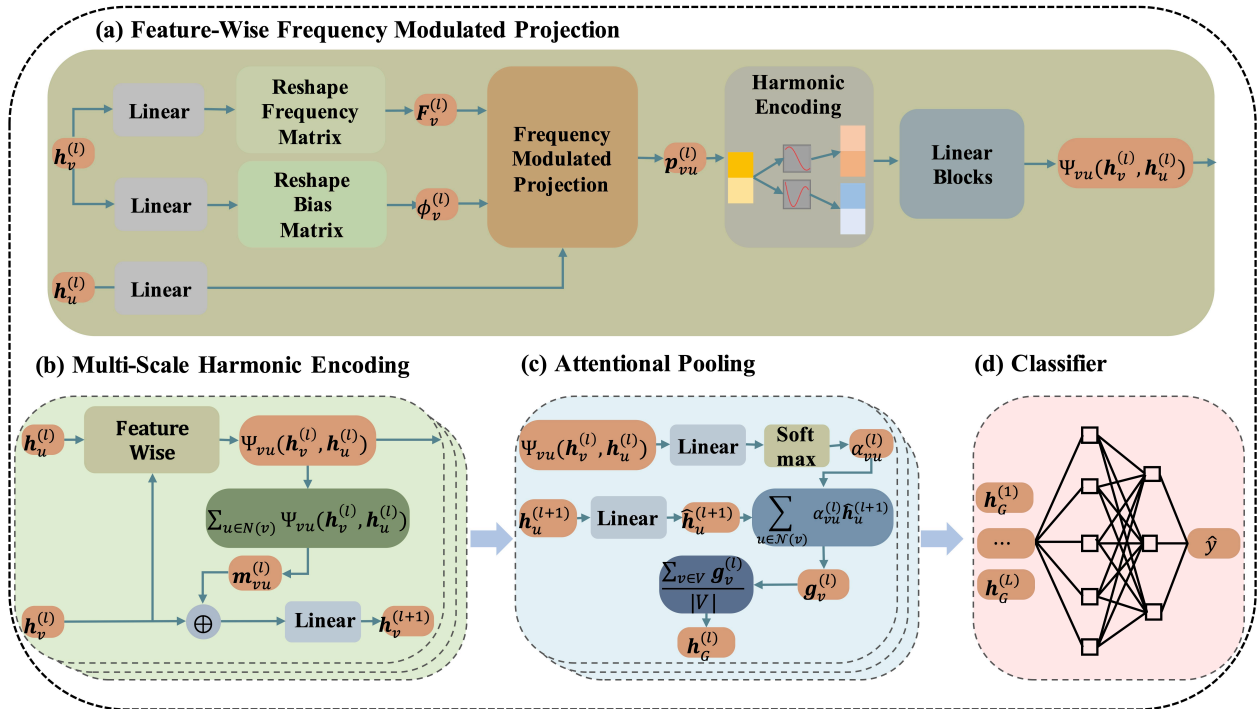


Figure 2: Overall architecture of the proposed **MSH-GNN** (Multi-Scale Harmonic Graph Neural Network). (a) *Feature-Wise Frequency Modulated Projection*: For each edge ($u \rightarrow v$), the target node v generates learnable frequency vectors and phase shifts to modulate the source node u 's features, producing frequency-aware edge embeddings via a Fourier expansion. (b) *Multi-Scale Harmonic Encoding*: Node-level message passing is guided by the frequency-modulated edge embeddings, enabling directional and feature-wise adaptive aggregation. (c) *Attentional Pooling*: Frequency-aware edge embeddings are used to compute attentional weights for aggregating local node representations into graph-level embeddings. (d) *Classifier*: Multi-scale graph-level features are fed into a multilayer perceptron for final prediction.

shaping. Graph-BERT [19] encodes spectral distances into input embeddings, but this remains static and is not updated during message passing.

By comparison, MSH-GNN integrates frequency modulation directly into the message function via sinusoidal encoding of directional projections. This enables dynamic, target-aware filtering during propagation and bridges the gap between token attention and local inductive biases.

2.3. Spectral and Kernel-Inspired Models

Spectral GNNs design filters in the frequency domain using the eigenspectrum of the graph Laplacian. Fourier-based models [16, 20] and WaveletNet [21] capture global structural patterns through fixed or learned spectral bases. However, these approaches generally operate over entire graphs or static eigenvectors, limiting their capacity to adapt to local structure or target-node preferences.

Kernel-based methods offer another line of expressiveness enhancement. GNTK [22] and other graph kernel models [23] encode graph similarity via fixed kernel functions or random feature mappings [24]. While theoretically sound, these models are typically non-parametric or detached from node-level learning, making them less practical for end-to-end graph representation learning.

Graph Neural Fields [20] use differential operators to capture smooth and oscillatory modes in spatiotemporal graphs.

Though powerful in modeling signal evolution, such frameworks operate on continuous fields rather than discrete node interactions, and lack learnable, edge-wise frequency modulation.

In contrast, MSH-GNN embeds harmonic modulation into message passing by applying multi-frequency sinusoidal functions over node-conditioned projections. This mechanism provides a localized, learnable approximation of kernel similarity, enabling fine-grained control over both spectral and structural cues.

2.4. Our Perspective

MSH-GNN is designed to unify and extend prior work along three complementary directions: message adaptivity, spectral encoding, and feature-wise filtering. Specifically, our model addresses the following gaps:

- **Lack of directional awareness**: Standard GNNs aggregate holistic neighbor embeddings, overlooking directional structure. We introduce *node-adaptive harmonic projection* to extract task-relevant feature directions.
- **Global-only frequency priors**: Spectral models rely on graph-wide eigenvectors and fixed encodings. In contrast, our *multi-scale modulation* is conditioned on target node context and applied during message construction.

- **Non-adaptive modulation:** FiLM-based and kernel-inspired methods apply static transformations. MSH-GNN performs *learnable, edge-level modulation* via sinusoidal expansion, achieving dynamic frequency selection and structural alignment.

To the best of our knowledge, MSH-GNN is the first framework to integrate node-specific harmonic basis projection with frequency-aware, multi-scale modulation. This architecture enables directional, feature-wise, and spectrally grounded message passing, offering a principled approach to enhancing GNN expressiveness in both structural and spectral domains.

3. Methods

3.1. MSH-GNN Architecture

We propose **MSH-GNN** (Multi-Scale Harmonic Graph Neural Network), a novel GNN architecture that performs *feature-wise adaptive message passing* with localized frequency modulation. Unlike conventional GNNs that treat neighbor embeddings as holistic vectors, MSH-GNN enables each node to extract task-relevant directional components from neighbors via node-specific basis projection and frequency-aware message modulation. Figure 2 illustrates the overall architecture, including: (1) feature-wise frequency modulated projection (node-adaptive projection layer, harmonic encoding module), (2) multi-scale harmonic modulation, and (3) frequency-aware attention pooling.

3.2. Node-Adaptive Projection Layer

Let $G = (V, E)$ be a graph with node features $\mathbf{h}_v \in \mathbb{R}^d$ for each node $v \in V$. At each layer l , node v adaptively generates a set of F frequency projection vectors and corresponding phase shifts using learnable linear projections:

$$\begin{aligned} \mathbf{F}_v^{(l)} &= \text{reshape}(\mathbf{W}_f \mathbf{h}_v^{(l)} + \mathbf{b}_f) \in \mathbb{R}^{F \times d}, \\ \boldsymbol{\phi}_v^{(l)} &= \mathbf{W}_\phi \mathbf{h}_v^{(l)} + \mathbf{b}_\phi \in \mathbb{R}^F. \end{aligned} \quad (1)$$

Here, $\mathbf{W}_f \in \mathbb{R}^{F \times d}$ and $\mathbf{b}_f \in \mathbb{R}^d$ are used to generate F frequency-aware projection vectors, reshaped into a matrix $\mathbf{F}_v^{(l)} \in \mathbb{R}^{F \times d}$. Similarly, $\mathbf{W}_\phi \in \mathbb{R}^{F \times d}$ and $\mathbf{b}_\phi \in \mathbb{R}^d$ produce a per-frequency phase shift vector $\boldsymbol{\phi}_v^{(l)}$.

For each edge ($u \rightarrow v$), the source node u 's features are projected under v 's frequency basis as:

$$\mathbf{p}_{vu}^{(l)} = \mathbf{F}_v^{(l)} \mathbf{h}_u^{(l)} + \boldsymbol{\phi}_v^{(l)} \in \mathbb{R}^F. \quad (2)$$

This frequency-modulated projection encodes the directional relevance of source node u to target node v under F adaptive filters, enabling feature-wise modulation in the subsequent message passing.

3.3. Harmonic Encoding Module

To nonlinearly enrich the directional projection $\mathbf{p}_{vu}^{(l)} \in \mathbb{R}^F$, we apply sinusoidal encoding over a set of predefined frequencies. Specifically, we define a set of K harmonic frequencies $\{\omega_k\}_{k=1}^K$ and compute:

$$\psi_k(\mathbf{p}_{vu}) = [\sin(\omega_k \mathbf{p}_{vu}) \parallel \cos(\omega_k \mathbf{p}_{vu})], \quad \omega_k \in \mathbb{R}. \quad (3)$$

In this work, we adopt an exponential schedule $\omega_k = 2^{k-1}$ for $k = 1, 2, 3$, corresponding to $\omega = \{1, 2, 4\}$. This captures both low- and high-frequency components and mimics the hierarchical frequency scaling used in positional encodings for Transformers [25]. This choice provides a balance between representational power and interpretability.

Alternative schedules such as linear $\omega_k = k$ or manually selected $\omega_k \in \{1, 3, 5\}$ were also tested, but did not yield consistent improvements. We note that ω_k can also be made learnable, either globally or conditioned on node pairs, which we leave as future work for further generalization.

This encoding scheme is reminiscent of random Fourier features [24], which approximate shift-invariant kernels via trigonometric projections. However, unlike randomly sampled bases, our method modulates node-specific projections \mathbf{p}_{vu} , resulting in localized and structure-aware embeddings.

Importantly, the concatenation of $\sin(\omega_k \cdot \mathbf{p}_{vu})$ and $\cos(\omega_k \cdot \mathbf{p}_{vu})$ across distinct ω_k values forms an injective map under mild regularity conditions, as supported by classical harmonic analysis. This ensures that directional differences in \mathbf{p}_{vu} are preserved after modulation.

The final modulated edge message is computed as:

$$\Psi_{vu}(\mathbf{h}_v^{(l)}, \mathbf{h}_u^{(l)}) = \mathbf{W}_o [\psi_1(\mathbf{p}_{vu}^{(l)}) \parallel \psi_2(\mathbf{p}_{vu}^{(l)}) \parallel \psi_3(\mathbf{p}_{vu}^{(l)})], \quad (4)$$

where \mathbf{W}_o is a learnable projection applied after Fourier expansion.

Kernel Interpretation. Our Fourier embedding module can be interpreted as a deterministic approximation of a shift-invariant kernel. Specifically, by applying multi-frequency sine and cosine transformations to the node-adaptive projections \mathbf{p}_{vu} , we implicitly map neighbor features into a high-dimensional Reproducing Kernel Hilbert Space (RKHS). This transformation is analogous to random Fourier features [24], but with structured and learnable frequency bases. It enables MSH-GNN to implement non-linear, target-aware similarity functions during message passing.

This perspective reveals that each message $\Psi_{vu}(\cdot)$ approximates a node-specific kernel function:

$$k_v(\mathbf{h}_u, \mathbf{h}_{u'}) \approx \psi(\mathbf{p}_{vu})^\top \psi(\mathbf{p}_{vu'}), \quad (5)$$

which allows fine-grained comparison across neighbor features. For formal derivation, see Appendix Appendix C.1.

Remark 1. *The harmonic encoding ψ_k implicitly embeds projected features into a Reproducing Kernel Hilbert Space (RKHS), endowing message functions with kernel-like structure.*

The details of Remark 1 can be found in Appendix Appendix C.1.

In summary, the entire message function of MSH-GNN between node v and u can be interpreted as an instance-specific kernel evaluation:

$$\begin{aligned} \Psi_{vu}(\mathbf{h}_v, \mathbf{h}_u) &\approx \mathbf{W}_o \cdot C(\mathbf{h}_u), \\ \text{with } k_v(\mathbf{h}_u, \mathbf{h}_{u'}) &= \langle C(\mathbf{h}_u), C(\mathbf{h}_{u'}) \rangle. \end{aligned} \quad (6)$$

where $C(\mathbf{h}_u) := [\psi_k(\mathbf{F}_v \mathbf{h}_u + \phi_v)]_k$ denotes the harmonic modulation of projected features. Here, C is the composition of a node-conditioned projection and multi-frequency harmonic encoding, resembling a deterministic Fourier feature map.

3.4. Directional Aggregation Layer

Node v aggregates frequency-modulated directional messages as:

$$\mathbf{m}_{vu}^{(l)} = \sum_{u \in N(v)} \Psi_{vu}(\mathbf{h}_v^{(l)}, \mathbf{h}_u^{(l)}), \quad \mathbf{h}_v^{(l+1)} = \text{MLP}(\mathbf{h}_v^{(l)} + \mathbf{m}_{vu}^{(l)}). \quad (7)$$

3.5. Frequency-Aware Attention Pooling

To generate graph-level representations, we apply a frequency-aware attention mechanism to modulated edge messages. For each node v , we compute edge-level attention weights and intermediate pooled features:

$$\begin{aligned} \alpha_{vu}^{(l)} &= \sigma(\mathbf{W}_1 \Psi_{vu}(\mathbf{h}_v^{(l)}, \mathbf{h}_u^{(l)})), \\ \mathbf{g}_v^{(l)} &= \sum_{u \in N(v)} \alpha_{vu}^{(l)} \cdot \mathbf{W}_2 \mathbf{h}_v^{(l+1)}, \end{aligned} \quad (8)$$

where $\mathbf{W}_1, \mathbf{W}_2$ are learnable parameters, and σ denotes a non-linear activation function (e.g., softmax or sigmoid) applied across edges.

The node-wise outputs are then averaged to form the layer-specific graph representation:

$$\mathbf{h}_G^{(l)} = \frac{1}{|V|} \sum_{v \in V} \mathbf{g}_v^{(l)}. \quad (9)$$

After L message passing layers, we perform a weighted combination of multi-layer representations to obtain the final graph embedding:

$$\mathbf{h}_G = \sum_{l=1}^L w_l \cdot \mathbf{h}_G^{(l)}, \quad (10)$$

where the weights w_l are learnable scalars trained to adaptively fuse information across different depths.

4. Theoretical Justification

Unlike simple Fourier positional embeddings used in Transformers, our harmonic map acts on node-conditioned projections, forming an adaptive kernel structure that varies per edge and target, beyond fixed or global encodings. We now analyze the expressive power of MSH-GNN from two complementary perspectives: (1) its equivalence to kernelized message functions; and (2) its ability to distinguish non-isomorphic graphs under the 1-Weisfeiler–Lehman (1-WL) test.

Kernel-based Expressiveness. The harmonic encoding module, by combining node-adaptive projections and multi-scale sinusoidal functions, implicitly defines a kernel k_v for each target node v , as discussed in Section 3. Specifically, each message takes the form:

$$\Psi_{vu}(\mathbf{h}_v, \mathbf{h}_u) = \mathbf{W}_o \cdot \psi(\mathbf{F}_v \mathbf{h}_u + \phi_v), \quad (11)$$

where $\mathbf{F}_v \in \mathbb{R}^{F \times d}$ and $\phi_v \in \mathbb{R}^F$ are learnable, node-specific projections derived from \mathbf{h}_v , and ψ is a multi-frequency harmonic map.

This can be interpreted as a deterministic approximation of a shift-invariant kernel:

$$k_v(\mathbf{h}_u, \mathbf{h}_{u'}) \approx \psi(\mathbf{p}_{vu})^\top \psi(\mathbf{p}_{vu'}), \quad \mathbf{p}_{vu} = \mathbf{F}_v \mathbf{h}_u + \phi_v. \quad (12)$$

The basis functions ψ resemble structured Fourier feature maps, and under sufficiently rich frequencies $\{\omega_k\}$, they enable MSH-GNN to approximate any continuous function over projected features [24, 26].

Combinatorial Expressiveness via 1-WL. To analyze the combinatorial expressiveness of MSH-GNN, we study its ability to distinguish non-isomorphic graphs under the 1-Weisfeiler–Lehman (1-WL) test. Unlike conventional GNNs that aggregate neighbor embeddings uniformly, MSH-GNN performs directional and frequency-modulated message passing, enabling more expressive multiset encodings.

Theorem 1 (Sufficient Conditions for 1-WL Expressiveness). *Let $\mathcal{F} : G \rightarrow \mathbb{R}^n$ be an instance of MSH-GNN. Suppose:*

- *Initial node features are distinguishable (e.g., injective or augmented with structural encodings);*
- *The projection \mathbf{F}_v and phase shift ϕ_v are generated via universal MLPs;*
- *The harmonic encoder ψ uses distinct, non-zero frequencies $\{\omega_k\}$;*
- *The aggregation and readout functions are permutation-invariant and sufficiently expressive (e.g., MLP).*

Then, \mathcal{F} is at least as powerful as the 1-WL test in distinguishing non-isomorphic graphs.

Remark 2. *Even when the assumptions above are only approximately satisfied (e.g., MLPs not perfectly injective), the harmonic projection and modulation still provide a strong inductive bias toward structure-aware neighborhood encoding. In practice, universal approximation and frequency separation ensure that MSH-GNN closely matches 1-WL behavior on real-world tasks.*

4.1. Computational Complexity

Let F be the frequency dimension and d the input size. For each edge, the cost of projection and modulation is $O(Fd)$. Given M edges and N nodes, the per-layer cost is: $O(MFd + NF^2)$. Thus, the total cost over L layers is: $O(L(MFd + NF^2))$. All operations are parallelizable on GPUs, and for small graphs (e.g., molecular datasets), this cost is negligible relative to transformer models.

4.2. Component Summary

MSH-GNN is composed of the following key modules:

- **Node-Adaptive Projection:** Learns node-conditioned direction filters \mathbf{F}_v and shifts ϕ_v ;
- **Multi-Scale Harmonic Modulation:** Applies sinusoidal encoding to directional projections across multiple frequencies ω_k ;
- **Frequency-Aware Attention Pooling:** Aggregates graph-level embeddings by emphasizing spectrally salient substructures.

These components jointly provide a frequency-aware, feature-wise message passing framework that is both expressive and interpretable.

5. Experiments

We assess the performance of MSH-GNN across diverse graph domains and tasks to verify its generality and frequency-aware design advantages. Our experiments address both node- and graph-level predictions, covering both graphs with regular substructures (e.g., molecular and protein graphs) and large-scale real-world graphs (e.g., social networks and synthetic benchmarks).

Our evaluation spans two key categories:

- **Motif-rich graphs**, including molecules and proteins from TU datasets (e.g., MUTAG, PTC, PROTEINS, NCI1), where symmetric and recurrent substructures (e.g., rings, chains, folds) are prevalent;
- **Real-world graphs**, such as social networks (e.g., IMDB-B, IMDB-M, RDT-B, COLLAB), where topological patterns are more diverse and less structured.

5.1. Baselines

We compare our proposed method MSH-GNN with a variety of baselines, including graph kernel methods, traditional and modern GNNs, and recent topological pooling architectures. Specifically, we include:

- **Graph Kernels:** to benchmark against non-learned baselines, including GNTK [22] and DCNN [27];
- **GNN-based Methods:** DGCNN [28], GIN [3], IGN [29], PPGNs [30], Natural GN [31], GSN [32], SIN [33], CIN [34], PIN [35] Dynamic Message Passing N^2 [36],
- **Pooling Methods:** to assess the effectiveness of our harmonic attention pooling against existing topological pooling approaches, such as GMT [37], SEP [38], Wit-TopoPool [39], GrePool [40] and RTPool [41]

5.2. Graph Classification

We follow the standard TU benchmark protocol using 10-fold cross-validation and report the mean accuracy with standard deviation. All baselines follow their original implementation settings. For datasets without node attributes (e.g., IMDB-B, IMDB-M, COLLAB), we adopt the common practice of encoding node degrees as one-hot vectors [3].

MSH-GNN consistently outperforms all baselines on structured datasets such as MUTAG, PTC, and PROTEINS, achieving up to 99.10% accuracy on MUTAG. These datasets are rich in biochemical motifs (e.g., aromatic rings, chain fragments), which exhibit strong periodicity or symmetry. We attribute our performance gains to the use of frequency-aware harmonic encoding, which enables MSH-GNN to better capture such recurring substructures compared to spatial or fixed spectral methods.

On larger and less structured datasets such as NCI1 and COLLAB, MSH-GNN maintains superior performance, outperforming both spectral and attention-based baselines (e.g., GMT, SEP). These results demonstrate that node-adaptive harmonic filters generalize well across both domain-specific and large-scale heterogeneous graphs. In contrast, pooling-based models such as Wit-TopoPool also perform competitively, but often require complex subgraph operations. MSH-GNN integrates similar inductive biases in a fully differentiable and lightweight framework.

5.3. Node Classification

To evaluate the generality of MSH-GNN beyond structured molecular graphs, we also conduct experiments on large-scale node classification datasets including CoauthorPhysics, AmazonPhoto, and Minesweeper. Full baseline comparisons are provided in Appendix Appendix D.1.

We adopt the same training setup as in [36], using public splits and average classification accuracy across multiple seeds. Results are summarized in Table 5.3.

As shown in Table 5.3, MSH-GNN achieves state-of-the-art performance across all four node classification benchmarks. Particularly on Minesweeper, a synthetic graph with planted motifs, our model surpasses N^2 by +0.81%, highlighting its advantage in capturing localized, frequency-sensitive patterns that elude conventional GNNs.

On real-world graphs like Amazon Photo and Coauthor Physics, where community structures and role-based patterns emerge, MSH-GNN benefits from harmonic attention that highlights structurally important nodes during readout. Unlike transformer-based models like Graphormer or GraphGPS, our model avoids overparameterization and out-of-memory (OOM) issues while still maintaining high accuracy.

5.4. Ablation Study

We conduct an ablation study to investigate the contribution of each component in MSH-GNN, including harmonic encoding, multi-scale frequency modulation, and pooling strategy. Results are summarized in Table 5.4.

Methods	MUTAG	PTC	PROTEINS	NCI1	IMDB-B	IMDB-M	RDT-B	COLLAB	
# Graphs	188	344	1113	4110	1000	1500	2000	5000	
Avg. Nodes	17.93	25.56	39.06	29.68	19.77	13.00	429.63	74.49	
Avg. Edges	19.79	26.96	72.82	32.13	96.53	65.94	497.75	2457.78	
# Classes	2	2	2	2	2	3	2	3	
Graph Kernels	GNTK [22]	90.0±8.5	67.9±6.9	75.6±4.2	84.2±1.5	76.9±3.6	52.8±4.6	N/A	83.6±1.0
	DCNN [27]	N/A	N/A	61.3±1.6	56.6±1.0	49.1±1.4	33.5±1.4	N/A	52.1±0.7
GNNs	DGCNN [28]	85.8±1.8	58.6±2.2	75.5±0.9	74.4±0.5	70.0±0.9	47.8±0.9	N/A	73.8±0.5
	IGN [29]	83.9±13.0	58.5±6.6	76.6±5.5	74.3±2.7	72.0±5.5	48.7±3.4	N/A	78.3±2.5
	GIN [3]	89.4±5.6	64.6±1.0	76.2±2.8	82.7±1.7	75.1±5.1	52.3±2.8	92.4±2.5	80.2±1.9
	PPGNs [30]	90.6±8.7	66.2±6.6	77.2±4.7	83.2±1.1	73.0±5.8	50.5±3.6	N/A	81.4±1.4
	Natural GN [31]	89.4±1.6	66.8±1.1	71.7±1.0	82.4±1.3	73.5±2.0	51.3±1.5	N/A	N/A
	GSN [32]	92.2±7.5	68.2±2.5	76.6±5.0	83.5±2.0	77.8±3.3	54.3±3.3	N/A	85.5±1.2
	SIN [33]	N/A	N/A	76.4±3.3	82.7±2.1	75.6±3.2	52.4±2.9	92.2±1.0	N/A
	CIN [33]	92.7±6.1	68.2±5.6	77.0±4.3	83.6±1.4	75.6±3.7	52.7±3.1	92.4±2.1	N/A
	PIN [35]	N/A	N/A	78.8±4.4	85.1±1.5	76.6±2.9	N/A	N/A	N/A
N ² [36]	N/A	N/A	77.53±1.78	83.52±3.75	79.95±2.46	57.31±2.19	N/A	86.72±1.62	
Pooling	GMT [37]	83.44±1.33	N/A	75.09±0.59	N/A	73.48±0.76	50.66±0.82	N/A	80.74±0.54
	SEP [38]	85.56±1.09	N/A	76.42±0.39	78.35±0.33	74.12±0.56	51.53±0.65	N/A	81.28±0.15
	Wit-TopoPool [39]	93.16±4.11	70.57±4.43	80.00±3.22	N/A	78.40±1.50	53.33±2.47	92.82±1.10	N/A
	GrePool [40]	86.25±8.35	59.86±6.67	N/A	82.13±1.57	N/A	50.77±3.25	N/A	81.42±1.53
	RTPool [41]	94.74±3.33	76.57±1.14	N/A	N/A	73.06±3.84	53.33±1.26	N/A	N/A
MSH-GNN (ours)	99.10±0.34	91.40±1.54	94.07±3.29	88.64±0.53	88.59±3.34	61.64±0.36	95.85±0.93	96.42±0.67	

Table 1: Graph classification results on TU datasets. The first section contains graph kernel methods, and the second section reports GNN-based methods. Results are mean classification accuracy (%) ± standard deviation.

Effect of Harmonic Encodinglogⁿl. Removing the harmonic encoding module results in substantial performance degradation, especially on PROTEINS and NCI1. This confirms the importance of frequency-aware message construction. Notably, static positional encodings such as LapPE and RWPE also improve performance, suggesting that spectral priors alone are beneficial. However, our *dynamic* harmonic encoding outperforms these static baselines, as it learns node-specific frequency filters that adapt to local structure.

Effect of Multi-Scale Sinusoidal Modulation. We further compare various choices of harmonic frequencies: *no modulation*, *single scale* ($K = 0$ or $K = 1$), *learned frequencies*, *linear schedule*, and *our default exponential schedule* ($\omega_k = 2^k$). We observe that multi-scale modulation consistently improves performance, with the exponential schedule achieving the best overall accuracy. Learned or linearly spaced frequencies yield suboptimal results, potentially due to instability or insufficient separation of harmonics.

Effect of Pooling Strategy. We compare three pooling strategies: mean, sum, and max pooling. Attention-based pooling consistently outperforms these naive methods, particularly on NCI1 and IMDB-B, where identifying structurally salient nodes is critical. This validates the importance of frequency-aware attention in the readout phase.

Summary. Unlike static Laplacian-based encodings (e.g., LapPE, RWPE), our harmonic module performs *target-adaptive projection* prior to modulation, enabling node-conditioned alignment of positional cues to the message context. This adaptive alignment mitigates potential misalignment

or over-smoothing induced by fixed encodings, and supports flexible, structure-aware representation learning across tasks.

6. Analysis and Interpretation

Beyond benchmark performance, we further analyze how MSH-GNN internally represents and responds to structural and spectral cues. We design a suite of diagnostic experiments to probe its behavior across frequency-structure classification, harmonic response visualization, and attention distribution dynamics.

6.1. Joint Frequency–Structure Classification

To rigorously evaluate the joint modeling capability of MSH-GNN in both structural and spectral domains, we design a synthetic classification task involving 30 distinct graph classes. Each class corresponds to a unique combination of graph topology and spectral frequency.

Graph Construction. We generate synthetic graphs from three structural families:

- **Ring graphs**: n -node cycle graphs with regular connectivity.
- **Chain graphs**: path graphs of the same size, exhibiting line-like topology.
- **Perturbed rings**: ring graphs with 20% of edges randomly rewired to introduce structural noise.

	CoauthorPhy	AmzPhoto	AmzComputers	Minesweeper
No. nodes	34,493	7,487	13,381	10,000
No. edges	247,962	119,043	245,778	39,402
GCN [1]	96.18±0.07	92.70±0.20	89.65±0.52	89.75±0.52
GAT [8]	96.17±0.08	93.87±0.11	90.78±0.17	92.01±0.68
GPRGNN [42]	96.85±0.08	94.49±0.14	89.32±0.29	86.24±0.61
APPNP [43]	96.54±0.07	94.32±0.14	90.18±0.17	-
GT [44]	97.05±0.05	94.74±0.13	91.18±0.17	91.85±0.76
Graphormer [12]	OOM	92.74±0.14	OOM	OOM
SAN [45]	OOM	94.86±0.10	89.83±0.16	-
GraphGPS [15]	OOM	95.06±0.13	OOM	92.29±0.61
NAG _{phormer} [46]	97.34±0.03	95.49±0.11	91.22±0.14	-
Expormer [47]	97.16±0.13	95.27±0.42	91.59±0.31	90.42±0.10
N ² [36]	97.56±0.28	95.75±0.34	92.51±0.13	93.97±0.27
MSH-GNN	98.37±0.08	97.66±0.50	92.84±1.61	94.78±0.64

Table 2: Node classification results on benchmark graphs (measured by accuracy: %).

Method Variant		MUTAG	PROTEINS	NCI1	IMDB-B
Harmonic Encoding	w/o Harmonic Encoding	92.19±0.66	77.71±0.32	71.58±0.28	72.48±0.41
	Static LapPE	89.89±1.47	80.00±1.35	86.81±1.72	83.72±0.88
	Static RWPE	99.04±0.57	92.27±0.68	83.41 ±0.74	86.64±0.43
Multi-Scale Sinusoids	w/o Multi-Scale	91.48±0.61	78.53±0.28	69.36±0.48	79.70±1.29
	$K = 0$	98.40±0.48	92.36±0.92	86.79±0.78	80.56±0.30
	$K = 1$	98.57±0.95	92.93±0.76	87.79±0.54	82.86±0.49
	Learned ω_k	91.74±0.38	88.62±0.54	87.14±0.49	81.75±0.29
Pooling Strategy	Linear ω_k	93.16±0.73	90.48±0.66	85.07±0.78	80.92±0.93
	Mean Pooling	98.99±0.50	91.08±0.86	87.51±0.47	86.58±0.39
	Sum Pooling	99.01±0.12	93.81±0.73	83.48±1.96	82.59±2.48
	Max pooling	98.40±0.62	89.93±1.02	87.90±0.94	84.20±1.14
MSH-GNN (Ours)		99.10±0.34	94.07±3.29	88.64±0.53	88.59±3.34

Table 3: Ablation results on representative TU datasets. We report accuracy (%) ± std. for different ablation settings.

Node Features. For each generated graph, we compute the unnormalized graph Laplacian $L = D - A$ and extract its eigenvectors $\lambda_0, \lambda_1, \dots, \lambda_{n-1}$. We then set the node features to be the k -th eigenvector λ_k , where $k \in \{0, 1, \dots, 9\}$. This eigenvector serves as a synthetic node signal with a well-defined spectral frequency: small k corresponds to low-frequency (smooth) signals, while large k represents high-frequency (oscillatory) signals.

Classification Task. Each graph is assigned a label indicating its *structure-frequency pair* (S, k) , where $S \in \{\text{ring, chain, perturbed}\}$ and k is the index of the chosen eigenvector. This results in a 30-class classification problem: 3 structural types \times 10 frequency levels. The goal is to predict the correct class label from the graph’s topology and node features.

Results. We compare three models: **GCN**, **GAT**, and our **MSH-GNN**. The per-class accuracy is visualized in Fig. 3, while efficiency and parameter statistics are summarized in Ta-

ble 6.2. **MSH-GNN** consistently outperforms others across all class types. In particular:

- **GCN** struggles to capture high-frequency signals and is sensitive to structural perturbations;
- **GAT** improves in low-frequency regions but fails to generalize across structural variants;
- **MSH-GNN** achieves robust performance across the entire spectrum, confirming its effectiveness in frequency-aware and structure-sensitive scenarios.

6.2. Scalability and Efficiency Analysis

We further assess the model complexity, inference cost, and GPU memory footprint during evaluation. As shown in Table 6.2, **MSH-GNN** requires only modest computational overhead compared to **GCN** and **GAT**, while achieving a significantly higher classification accuracy on this frequency-structure task.

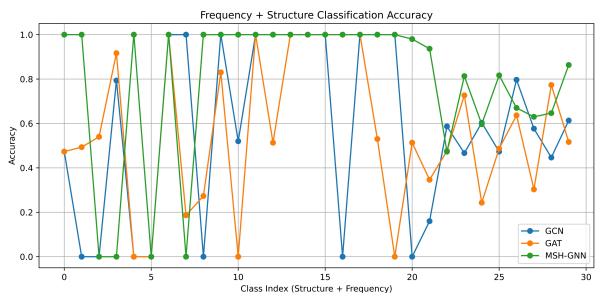


Figure 3: Per-class accuracy on frequency + structure classification. Classes 0–9 are ring graphs, 10–19 are chains, and 20–29 are perturbed rings. MSH-GNN shows strong generalization across both frequency and structural variations.

Model	#Params	Inference (s)	GPU (MB)	Accuracy
GCN	6.2K	1.40	17.90	0.5837
GAT	6.5K	2.50	17.95	0.5593
MSH-GNN	7.3K	2.74	26.64	0.7809

Table 4: Model complexity and efficiency comparison on the synthetic classification task.

6.3. Structure-Frequency Representation Analysis

To further investigate whether MSH-GNN captures discriminative information regarding both structural type and spectral frequency, we conduct a post-hoc visualization experiment. Specifically, we extract the graph-level harmonic responses from the first convolutional layer of MSH-GNN after message passing, where each graph is represented by the aggregated frequency response over its nodes.

We compare MSH-GNN against GCN and GAT under the same task: classifying synthetic graphs constructed from ring, chain, and perturbed-ring structures, each annotated with a dominant frequency index. For each model, we compute graph-wise representations and project them to 2D using t-SNE [48].

As shown in Figure 4, MSH-GNN produces more clearly clustered embeddings, with different structure-frequency combinations forming distinguishable groups. In contrast, GCN and GAT exhibit much more entangled distributions, indicating weaker capacity to differentiate structure-frequency patterns. This result supports that MSH-GNN’s frequency-aware harmonic encoding effectively enhances representation learning over graphs with varying spectral properties.

6.4. Attention Distribution Analysis

To better understand how MSH-GNN distinguishes graph structures during pooling, we visualize the learned attention weights α_{uv} assigned by our Attentional Pooling module. Figure 5 shows the attention distributions for edges from ring, chain, and perturbed ring graphs, respectively.

We observe that attention values in ring graphs are sharply peaked around certain edges, suggesting the model selectively focuses on structurally aligned motifs. Chain graphs show a moderately dispersed attention distribution, while perturbed rings exhibit the flattest profile, indicating more uniform edge

weighting due to structural disorder. This aligns with our intuition: harmonic attention learns to emphasize structurally consistent or repetitive substructures, and adaptively relaxes its focus when input graphs are irregular or noisy.

These results highlight that MSH-GNN not only captures frequency-domain signals but also dynamically adjusts its attention strategy based on the underlying structure, contributing to its robust generalization across domains.

Together, these analyses confirm that MSH-GNN not only achieves strong predictive performance, but also learns interpretable, structure-aware representations that generalize across spectral variations.

6.5. Case Study: Interpretable Analysis of Org12692

To evaluate the interpretability of our model, we perform a case study on a representative molecule from the BBBP dataset with the SMILES string FC(F)(F)c1c(Cl)nc(N2CCNCC2)cc1, known as Org12692. This compound features a trifluoromethyl group (CF_3), a chloro-substituted aromatic ring, and a piperazine moiety—structural motifs that are known to influence blood–brain barrier (BBB) permeability. We employ GNNExplainer [49] to extract both node-level and feature-level saliency for GCN, GAT, and our proposed MSH-GNN models trained on the BBBP classification task. The interpretability analysis procedure is outlined in Appendix Appendix E.

Node-level saliency. The saliency scores are visualized using MolView, where warmer colors indicate higher attribution to the prediction.

Among all models, MSH-GNN provides the most focused and chemically coherent importance map. It distinctly identifies fluorine (F), chlorine (Cl), and heteroatoms in aromatic rings as highly influential—regions strongly associated with BBB permeability. In contrast, GCN and GAT generate more diffuse and less interpretable saliency distributions.

These results demonstrate that the frequency-aware and directionally modulated message passing in MSH-GNN not only improves classification performance, but also enhances post-hoc interpretability by aligning model attention with chemically meaningful substructures.

Feature-Level Attribution Analysis. To investigate which atomic descriptors most influence model predictions, we compute feature-wise saliency for the Org12692 molecule in the BBBP dataset. As shown in Figure 7, we calculate input gradients with respect to atomic features and aggregate them across all nodes to yield mean importance scores.

The results show that MSH-GNN assigns higher importance to interpretable descriptors such as electronegativity (χ), atomic radius (atom_rad), and valence shell occupancy (nsvalence , npvalence). These properties partially reflect atomic polarity and spatial profile, which are known to influence blood–brain barrier (BBB) permeability. In contrast, GCN and GAT distribute saliency more uniformly across features, suggesting weaker alignment with chemically relevant inductive biases.

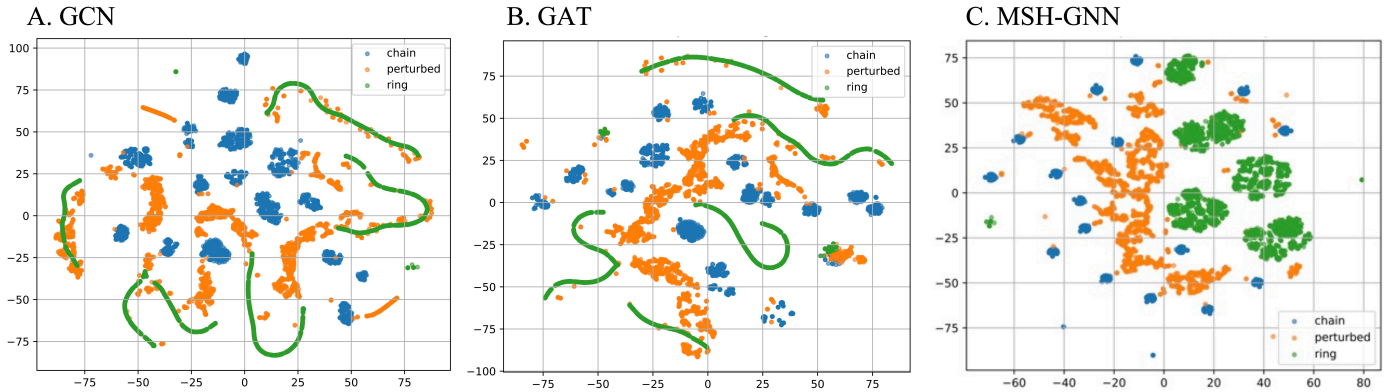


Figure 4: Graph-level embedding visualization via t-SNE. Each point represents one graph, colored by structural type (ring / chain / perturbed). MSH-GNN produces more separable clusters, indicating better structure–frequency representation.

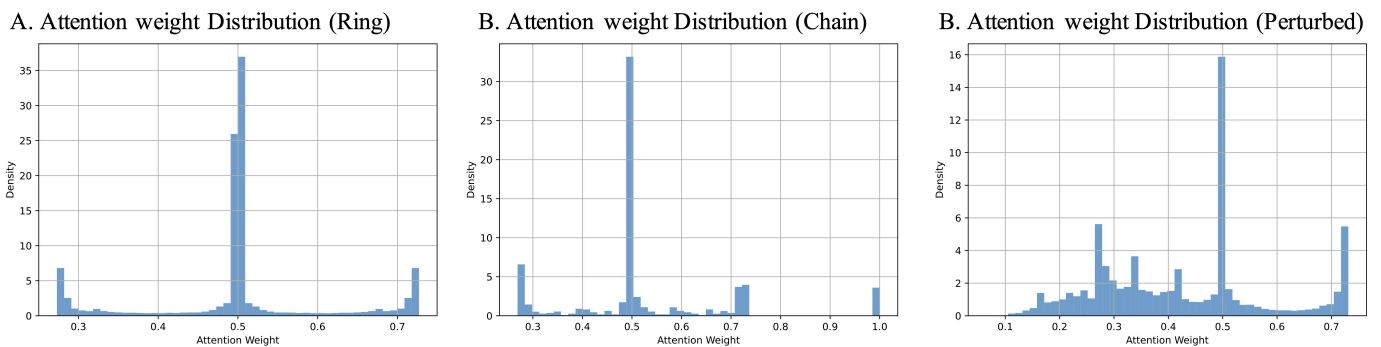


Figure 5: Distributions of attention weights α_{wv} learned by Attentional Pooling on graphs of different structural types. Ring graphs induce more focused attention patterns than perturbed ones.

This highlights that the **frequency-aware modulation** in MSH-GNN helps it focus on semantically meaningful attributes, thereby enhancing both predictive accuracy and interpretability.

6.6. Quantitative Evaluation of Model Interpretability

Following prior work [50], we adopt Gini index and entropy to evaluate the sparsity and complexity of model explanations. Higher Gini values indicate more focused attribution on a small subset of nodes, whereas lower entropy suggests more concise and interpretable feature usage. Detailed metric definitions are provided in Appendix Appendix F.

As shown in Table 5, MSH-GNN achieves the highest predictive performance (AUC = 0.631), while maintaining a desirable trade-off between attribution concentration (Gini = 0.372) and entropy (2.3960). GAT achieves the most concentrated saliency (Gini = 0.502) and the lowest entropy (2.3952), suggesting highly sparse and focused explanations, albeit with slightly lower accuracy (AUC = 0.591). GCN performs the worst in both accuracy and interpretability.

These results indicate that MSH-GNN balances predictive power and interpretability, benefiting from its frequency-aware, directionally modulated message passing scheme.

Table 5: Interpretability metrics on Org12692. Higher Gini and lower Entropy indicate more focused attribution.

Model	AUC \uparrow	Gini \uparrow	Entropy \downarrow
GCN	0.571	0.156	2.3967
GAT	0.591	0.502	2.3952
MSH-GNN	0.631	0.372	2.3960

7. Conclusion and Future Work

We presented MSH-GNN, a novel graph neural network architecture that integrates node-specific harmonic projections with multi-scale sinusoidal modulation for frequency-aware, feature-wise message passing. By encoding directional and spectral inductive biases directly into the message construction process, MSH-GNN enables fine-grained selection of task-relevant features from neighbors, significantly enhancing the model’s expressiveness compared to conventional GNNs that treat node embeddings as holistic vectors.

From a theoretical perspective, we show that our harmonic encoding acts as a kernel approximation, endowing message functions with nonlinear, structure-adaptive filtering properties. We further prove that MSH-GNN matches the expressive power of the 1-Weisfeiler–Lehman test under mild injectivity conditions, while functioning as a frequency-selective operator over

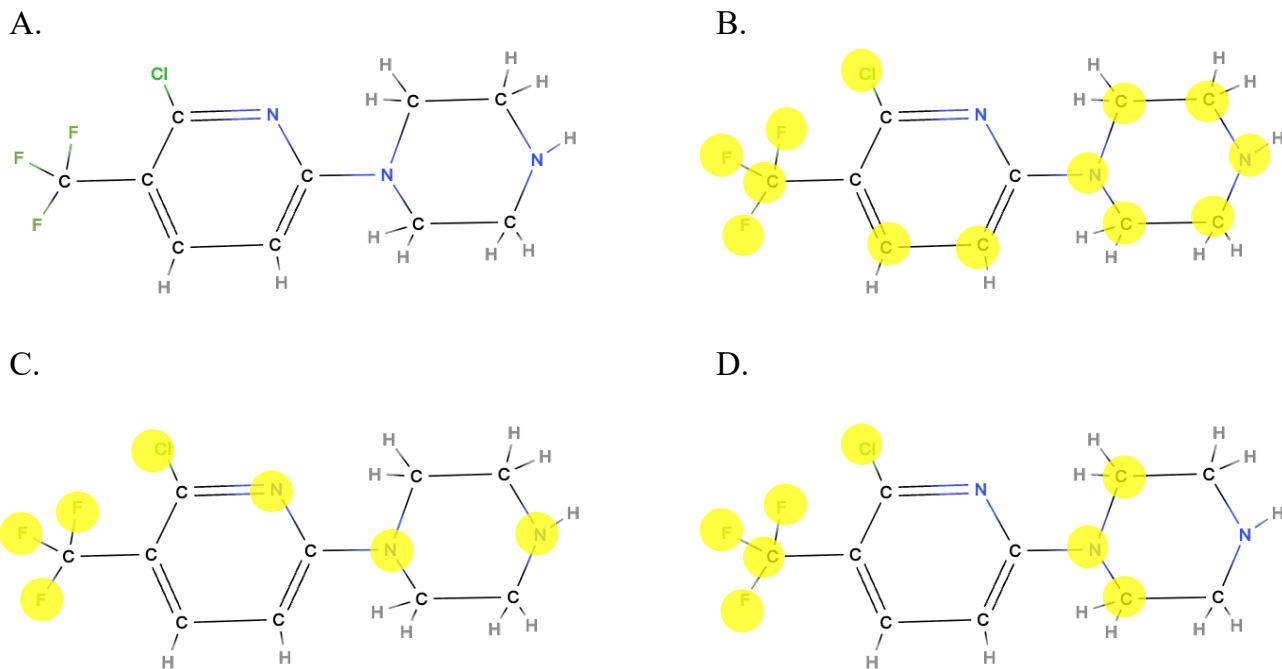


Figure 6: Visualization of node importance for the molecule Org12692 in the BBBP dataset. (A) Original molecule visualized using MolView. (B) Node saliency map generated by GCN. (C) Node saliency map generated by GAT. (D) Node saliency map generated by MSH-GNN, highlighting chemically meaningful substructures such as the CF₃ group and heteroaromatic ring. Warmer colors indicate higher saliency. MSH-GNN provides more localized and interpretable explanations aligned with known pharmacophores.

graph signals.

Empirically, MSH-GNN achieves state-of-the-art performance across both molecular and social graph benchmarks, with consistent gains in classification accuracy. Notably, in our synthetic *Analysis and Interpretation*, MSH-GNN demonstrates strong generalization across both topological and spectral variations, outperforming GCN and GAT by large margins.

To further interpret its behavior, we visualize graph-level harmonic responses using t-SNE, revealing clearly separable clusters corresponding to different structure-frequency pairs. Combined with attention heatmaps, these analyses confirm that MSH-GNN not only performs well but also learns structured, discriminative representations aligned with spectral semantics.

Future directions include extending our framework to: (i) support equivariant or invariant designs under geometric transformations; (ii) incorporate adaptive or learnable frequency scales; and (iii) explore hierarchical or subgraph-level spectral modeling to enhance compositionality and interpretability.

Overall, MSH-GNN bridges spectral graph theory and neural message passing, offering a principled and scalable foundation for frequency-aware graph learning. We believe it opens up new avenues for modeling structural signals in physical, biological, and scientific domains.

Appendix A. Appendix Overview

This appendix provides additional theoretical and empirical details to support our main claims. In Appendix Appendix B, we construct a counterexample showing that MSH-GNN can

distinguish graphs that GAT cannot. Appendix Appendix C.1 formally derives the harmonic encoding as a kernel approximation and spectral filter. Appendix Appendix C.3 presents a 1-WL expressiveness analysis. Finally, we detail experimental setups and hyperparameters in Appendix Appendix D.1.

Appendix B. Constructive Example: Distinguishing MSH-GNN from GAT

To highlight the expressiveness advantage of MSH-GNN over attention-based GNNs, we construct a pair of graphs G_1 and G_2 that are indistinguishable by GAT but clearly separable by MSH-GNN.

Consider two star graphs shown in Figure 1, each with a central node v and three neighbors u_1, u_2, u_3 . Both graphs satisfy:

- The same central node feature: $\mathbf{h}_v = [0, 0]$;
- The same mean of neighbor features: $\frac{1}{3}(\mathbf{h}_{u_1} + \mathbf{h}_{u_2} + \mathbf{h}_{u_3}) = [0.67, 0.67]$;
- But distinct directional arrangement of neighbor features.

GAT Cannot Distinguish G_1 and G_2 . GAT computes scalar attention scores α_i based on the compatibility between h_v and h_{u_i} , and performs the following aggregation:

$$\mathbf{h}'_v = \sum_{i=1}^3 \alpha_i \mathbf{h}_{u_i}, \quad \sum_i \alpha_i = 1.$$

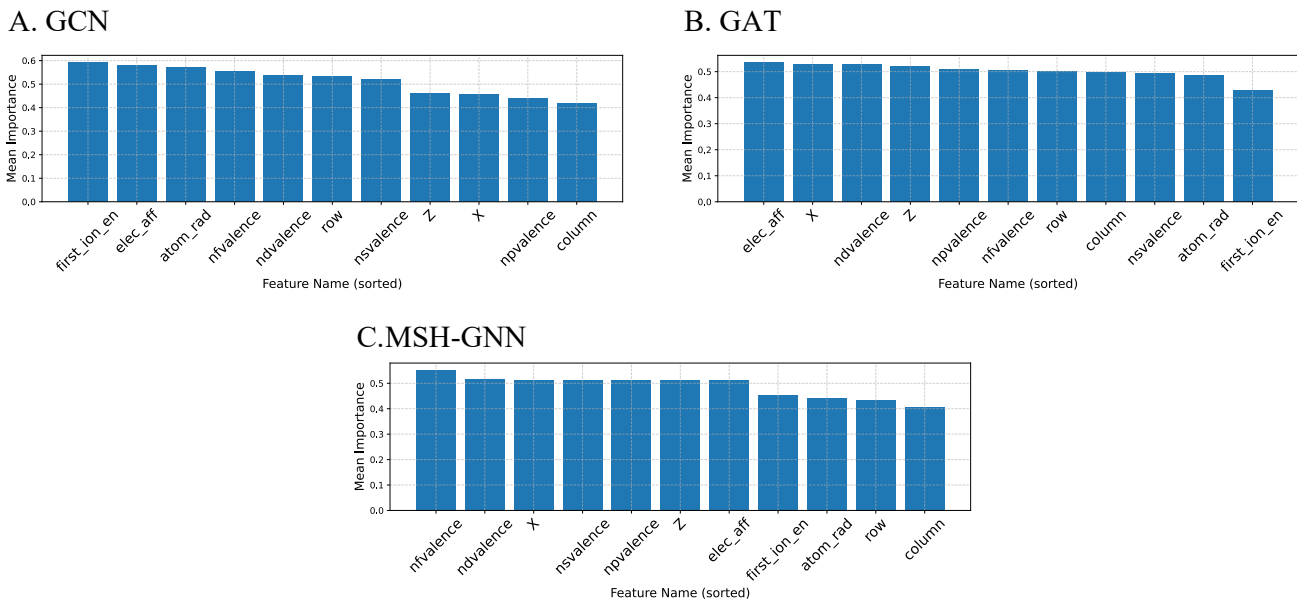


Figure 7: Feature-wise importance for Org12692 in the BBBP dataset, averaged over all atoms. Saliency scores are computed using input gradients. **MSH-GNN** assigns higher attribution to interpretable atomic descriptors such as electronegativity (X), atomic radius (atom_rad), and valence shell features (nvalence, npvalence). These features relate to polarity and electronic configuration, which are known to influence blood-brain barrier permeability. In contrast, GCN and GAT produce more diffuse attribution across features, suggesting weaker selectivity.

Since the average neighbor feature is the same and $h_v = [0, 0]$, GAT produces similar outputs for G_1 and G_2 . It lacks the capacity to differentiate directional arrangements or intra-feature asymmetry.

MSH-GNN Captures Directional Differences. In contrast, MSH-GNN modulates messages using target-dependent projections and multi-scale harmonics:

$$\begin{aligned} \mathbf{p}_{vu} &= \mathbf{F}_v \mathbf{h}_u + \phi_v, \\ \psi_k(\mathbf{p}_{vu}) &= \sin(2^k \mathbf{p}_{vu}) \parallel \cos(2^k \mathbf{p}_{vu}), \\ \Psi_{vu}(\mathbf{h}_v, \mathbf{h}_u) &= \mathbf{W}_o [\psi_1(\mathbf{p}_{vu}) \parallel \psi_2(\mathbf{p}_{vu}) \parallel \psi_3(\mathbf{p}_{vu})]. \end{aligned}$$

Even if neighbor averages are equal, the node-specific projections $\mathbf{F}_v \mathbf{h}_u$ preserve directional information, and harmonic modulation accentuates these differences at multiple frequency scales. As a result, Ψ_{vu} differs between G_1 and G_2 despite equal mean inputs, enabling MSH-GNN to distinguish the graphs. Therefore, MSH-GNN distinguishes G_1 and G_2 via:

- Direction-sensitive basis projection;
- Phase-aware modulation;
- Nonlinear frequency filtering that breaks permutation symmetry in feature space.

This example illustrates the failure of GAT under structural aliasing and the power of MSH-GNN to overcome it via feature-wise, frequency-aware message construction.

Appendix C. Theoretical Justification

Appendix C.1. Appendix: Harmonic Modulation as Kernel Approximation

We now show that the harmonic modulation in MSH-GNN can be interpreted as an approximation of a shift-invariant kernel. This connection provides theoretical insight into the model’s ability to learn rich, non-linear feature interactions.

Appendix C.1.1. Bochner’s Theorem and Random Fourier Features

Bochner’s theorem states that a continuous, shift-invariant kernel $k(x, x') = k(x - x')$ on \mathbb{R}^d is positive definite if and only if it is the Fourier transform of a non-negative finite measure:

$$k(x - x') = \int_{\mathbb{R}^d} e^{i\eta^\top(x-x')} d\mu(\eta).$$

When μ is absolutely continuous with respect to the Lebesgue measure, it has a density $p(\eta)$, and we can write:

$$k(x - x') = \mathbb{E}_{\eta \sim p} [e^{i\eta^\top x} e^{-i\eta^\top x'}].$$

Using Euler’s identity and Monte Carlo approximation, we obtain the random Fourier feature (RFF) map:

$$z(x) = \sqrt{2} \cos(\eta^\top x + b),$$

with $\eta \sim p(\eta)$, $b \sim \text{Uniform}[0, 2\pi]$. Then,

$$k(x, x') \approx z(x)^\top z(x').$$

Appendix C.1.2. MSH-GNN's Harmonic Encoding as Deterministic Fourier Features

Recall from Section 3 that each node v generates a frequency projection matrix $\mathbf{F}_v \in \mathbb{R}^{F \times d}$ and a phase shift vector $\phi_v \in \mathbb{R}^F$. For each edge (v, u) , the modulated projection is computed as:

$$\mathbf{p}_{vu} = \mathbf{F}_v \mathbf{h}_u + \phi_v,$$

and is further encoded via multiple frequencies ω_k as:

$$\psi(\mathbf{p}_{vu}) = \prod_{k=0}^K [\sin(\omega_k \mathbf{p}_{vu}) \parallel \cos(\omega_k \mathbf{p}_{vu})].$$

This encoding scheme is equivalent to a deterministic version of random Fourier features, where:

- The input \mathbf{h}_u is first projected through node-specific direction \mathbf{F}_v and shifted by ϕ_v ;
- The frequencies $\omega_k = 2^{k-1}$ are fixed exponentially;
- The resulting feature $\psi(\mathbf{p}_{vu})$ is used as the basis for message passing.

Therefore, we can view MSH-GNN's harmonic modulation as a structured, target-dependent approximation of a shift-invariant kernel:

$$k_v(\mathbf{h}_u, \mathbf{h}_{u'}) \approx \psi(\mathbf{p}_{vu})^\top \psi(\mathbf{p}_{vu'}),$$

where ψ acts as a deterministic feature map into a Reproducing Kernel Hilbert Space (RKHS).

This kernel-like property enables the model to encode nonlinear similarities across neighbor features in a localized and adaptive fashion. Injectivity and universal approximation of such harmonic maps follow from Barron's Theorem [26], which states that sinusoidal bases with structured frequencies can approximate any bounded continuous function on compact domains in L^2 norm.

Remark 3. *Unlike random Fourier features which are globally sampled, MSH-GNN learns node-specific structured projections, enabling localized, target-conditioned nonlinear filters. This improves over global spectral encoding models [16].*

Appendix C.2. Spectral Modulation and Frequency Selectivity

GCN applies the same convolutional weight to all frequency components, while GAT attends to nodes but not spectral modes. In contrast, MSH-GNN applies different modulations ψ_k to each projected signal, selectively amplifying frequency components based on learned filters \mathbf{F}_v and ϕ_v .

We now analyze how the harmonic modulation mechanism in MSH-GNN responds to graph signals of different frequencies. Specifically, we show that sinusoidal modulation combined with node-adaptive projection acts as a *frequency-selective filter* over the graph spectrum.

Spectral Setting. Consider a graph $G = (V, E)$ with normalized Laplacian matrix $L \in \mathbb{R}^{n \times n}$, whose eigenvectors $\{\lambda_k\}_{k=1}^n$ form a complete orthonormal basis for signals on the graph. A node feature matrix $H \in \mathbb{R}^{n \times d}$ can be decomposed spectrally as:

$$H = \sum_{k=1}^n \lambda_k \lambda_k^\top H = \sum_{k=1}^n \hat{H}_k,$$

where $\hat{H}_k := \lambda_k \lambda_k^\top H$ denotes the k -th frequency component.

Modulation as Frequency Filter. For a node v and neighbor u , the harmonic message is:

$$\begin{aligned} \mathbf{p}_{vu} &= \mathbf{F}_v \mathbf{h}_u + \phi_v, \\ \psi(\mathbf{p}_{vu}) &= \prod_{k=0}^K [\sin(\omega_k \mathbf{p}_{vu}) \parallel \cos(\omega_k \mathbf{p}_{vu})]. \end{aligned}$$

where \mathbf{F}_v is learned from h_v , and $\omega_k = 2^k$ are fixed frequencies.

This operation can be seen as applying a frequency-dependent nonlinearity on the projected signal:

- Low-frequency components (smooth signals) vary slowly and align with low ω_k .
- High-frequency components (local variations, e.g., boundaries or irregularity) induce rapid oscillations and are emphasized by higher ω_k .

Spectral Selectivity. Let $h_u = \lambda_k$, i.e., the k -th Laplacian eigenvector. Then:

$$\mathbf{p}_{vu} = \mathbf{F}_v \mathbf{h}_u + \phi_v, \quad \psi(\mathbf{p}_{vu}) = \text{sinusoids of } \lambda_k.$$

Hence, ψ retains information about frequency index k via the argument $\omega_k \lambda_k$, producing distinguishable responses per ϕ_k .

This proves that MSH-GNN possesses *frequency selectivity*, i.e., it can differentiate and encode input signals based on their spectral content. This property is absent in conventional GNNs (e.g., GCN, GIN), which apply the same transformation across all frequencies.

Remark 4. *MSH-GNN encodes frequency via learnable projection and harmonic modulation, acting as a localized, multi-band filter bank on graph signals.*

Appendix C.3. Expressiveness of MSH-GNN

In contrast to the more practical Theorem 1 in the main text, here we formalize a stricter version of expressiveness under fully injective conditions.

Theorem 2 (Injective Message Functions Implies 1-WL Expressiveness). *Let $\mathcal{F} : G \rightarrow \mathbb{R}^n$ be an instance of MSH-GNN. Suppose that:*

- *the initial node features are injective (or augmented with unique identifiers / structural encodings);*
- *the frequency projection \mathbf{F}_v and phase shifts ϕ_v are derived via injective MLPs from \mathbf{h}_v ;*

- the harmonic map $\psi(\cdot)$ uses linearly independent frequencies $\{\omega_k\}$;
- the attention readout $\sigma(\mathbf{W}_1 \cdot)$ is injective.

Then \mathcal{F} is at least as powerful as the 1-Weisfeiler–Lehman (1-WL) test in distinguishing non-isomorphic graphs.

Proof. We follow the injectivity framework in [3]. In MSH-GNN, the edge message from u to v is computed as:

$$\begin{aligned} \mathbf{p}_{vu} &= \mathbf{F}_v \mathbf{h}_u + \phi_v, \\ \psi_k(\mathbf{p}_{vu}) &= [\sin(\omega_k \mathbf{p}_{vu}) \parallel \cos(\omega_k \mathbf{p}_{vu})] \\ \Psi_{vu}(\mathbf{h}_v, \mathbf{h}_u) &= \mathbf{W}_o \cdot \left[\parallel_{k=0}^K \psi_k(\mathbf{p}_{vu}) \right]. \end{aligned}$$

Since \mathbf{F}_v , ϕ_v are obtained from an injective transformation of \mathbf{h}_v , and $\{\omega_k\}$ are linearly independent, the composed map Ψ_{vu} is injective in \mathbf{h}_u conditioned on \mathbf{h}_v .

Let $\mathcal{N}(v)$ and $\mathcal{N}(v')$ be two neighborhoods with different multisets of features. Then, the sets $\{\Psi_{vu}(\cdot)\}_{u \in \mathcal{N}(v)}$ and $\{\Psi_{v'u'}(\cdot)\}_{u' \in \mathcal{N}(v')}$ will differ under multiset aggregation (e.g., summation or mean), provided the underlying set of messages differs.

Finally, MSH-GNN updates \mathbf{h}_v via:

$$\mathbf{h}_v^{(l+1)} = \text{MLP} \left(\mathbf{h}_v^{(l)} + \sum_{u \in \mathcal{N}(v)} \Psi_{vu}(\mathbf{h}_v^{(l)}, \mathbf{h}_u^{(l)}) \right),$$

which preserves injectivity under standard conditions. The attention pooling mechanism is also injective, given that $\alpha_{vu} = \sigma(\mathbf{W}_1 \mathbf{m}_{vu})$ is computed from an injective map over messages.

Hence, MSH-GNN implements an injective update and readout over neighborhoods and the graph, satisfying the conditions for matching 1-WL expressiveness. \square

Remark 5. *Injectivity of the harmonic encoding ψ holds under mild conditions, such as distinct ω_k spanning \mathbb{R}^F , and MLPs with sufficient capacity. Thus, MSH-GNN is theoretically capable of distinguishing non-isomorphic graphs that 1-WL can separate, and provides stronger inductive bias for frequency-sensitive patterns.*

By embedding neighbors in a structured sinusoidal space, MSH-GNN enhances the expressiveness of message passing with localized, frequency-aware filters. The kernel perspective provides both a theoretical justification and an interpretation of the harmonic encoding as an inner-product in an implicit high-dimensional space.

Appendix D. Supplementary of Experiments settings

Appendix D.1. Node Classification

To evaluate the generality of our proposed MSH-GNN beyond graph-level prediction tasks, we further conduct experiments on benchmark node classification datasets, including Coauthor Physics, Amazon Computers, Amazon Photo, and Minesweeper.

These datasets cover co-authorship, e-commerce, and synthetic graphs with varying levels of structural regularity. We follow the training setup of [36], using public splits and average accuracy over multiple seeds.

Baselines. We compare against representative GNNs and transformer-based graph models:

- **Message Passing GNNs:** GCN [1], GAT [8], APPNP [43], GPR-GNN [42];
- **Graph Transformers:** GT [44], Graphormer [12], SAN [45], GraphGPS [15];
- **Spectral-aware Transformers:** NAG_{phormer} [46], EXphormer [47], N² [36].

Appendix D.2. Hyperparameter Settings

We apply grid search to tune the key hyperparameters for each dataset. The final selected configurations are reported in Table Appendix D.2. For all experiments, the optimizer is Adam with a learning rate of 0.001, and dropout is set to 0.1. We use hidden dimension 64 and output dimension 16 unless otherwise stated.

Dataset	#Layers	Hidden_1	Hidden_2	Dropout
TU datasets	3	64	16	0.1
CoauthorPhysics	3	64	16	0.1
AmazonComputers	3	64	16	0.1
AmazonPhoto	3	64	16	0.1
Minesweeper	15	64	16	0.1

Table D.6: Hyperparameter settings for each dataset.

Hardware Environment. All experiments were conducted on a server equipped with:

- **CPU:** Intel(R) Xeon(R) Gold 5318Y @ 2.10GHz
- **GPU:** 2 × NVIDIA A30 (24GB each)
- **CUDA Version:** 12.2
- **Driver Version:** 535.104.05
- **OS:** Linux (Ubuntu 20.04)

Appendix E. Explanation Protocol for BBBP Molecules

To analyze the interpretability of GNN models on the BBBP dataset, we adopt a saliency-based post-hoc explanation strategy on trained classifiers. The procedure is as follows:

Dataset and Sample. We use the BBBP dataset, where each graph corresponds to a molecule represented via SMILES. For interpretability, we select the molecule **Org12692** with SMILES FC(F)(F)c1c(C1)nc(N2CCNCC2)cc1, known to have BBB permeability. Each SMILES string is converted to a graph via RDKit, with 11-dimensional atomic features including period, group, electronegativity, etc.

Mathematical Formulation of Attribution Scores. Formally, we quantify the importance of each node and feature dimension using input gradients and learned masks.

Node-level saliency. We define the saliency score for a node v as the L_1 norm of the gradient of the model output \hat{y} with respect to the input features $\mathbf{h}_v \in \mathbb{R}^d$:

$$\text{Saliency}(v) = \left\| \frac{\partial \hat{y}}{\partial \mathbf{h}_v} \right\|_1 = \sum_{i=1}^d \left| \frac{\partial \hat{y}}{\partial h_{v,i}} \right|.$$

This measures the overall sensitivity of the prediction to perturbations at node v .

Feature-level attribution. To assess which atomic descriptors most influence the prediction, we apply a learnable mask $\mathbf{s} \in \mathbb{R}^{|V| \times d}$ to the input features $\mathbf{h}_v \in \mathbb{R}^d$. The masked input is defined as:

$$\tilde{\mathbf{h}}_v = \mathbf{h}_v \odot \sigma(\mathbf{s}_v),$$

where $\sigma(\cdot)$ denotes the sigmoid function applied element-wise to the trainable mask.

The mask is optimized to minimize the discrepancy between the prediction on the masked graph and the original output:

$$\mathcal{L} = \left(\hat{y}(\tilde{\mathbf{X}}, \mathcal{G}) - \hat{y}(\mathbf{X}, \mathcal{G}) \right)^2.$$

The final importance score for feature dimension i is computed as the mean mask activation across all nodes:

$$\text{Importance}(i) = \frac{1}{|V|} \sum_{v \in V} \sigma(m_{v,i}).$$

This approach allows us to compare model interpretability in identifying functional groups (e.g., halogens, piperazine ring) relevant to BBB classification.

Appendix F. Quantitative Interpretability Metrics

To quantitatively evaluate model interpretability, we adopt two standard metrics—Gini index and entropy—that have been used in prior work to assess the sparsity and complexity of explanations, respectively [50]. The Gini index captures how concentrated the attribution is over a small set of elements, while entropy measures how evenly importance scores are distributed.

Gini Index. For a node-level saliency vector $\mathbf{s} \in \mathbb{R}^n$, where $s[v] = \text{Saliency}(v)$ for node $v \in V$ and $|V| = n$, the Gini index [51] is computed as:

$$\text{Gini}(\mathbf{s}) = \frac{\sum_{u \in V} \sum_{v \in V} |\mathbf{s}[u] - \mathbf{s}[v]|}{2n \sum_v \mathbf{s}[v]}.$$

A higher Gini index indicates more concentrated attribution on a small set of influential nodes.

Entropy. For a feature-level importance vector $\mathbf{I} \in \mathbb{R}^d$, where $\mathbf{I}[i] = \text{Importance}(i)$ for each dimension i , we assess the uniformity of feature usage using the normalized Shannon entropy [52]:

$$\text{Entropy}(\mathbf{I}) = - \sum_{i=1}^d \tilde{f}_i \log \tilde{f}_i, \quad \tilde{f}_i = \frac{\mathbf{I}[i]}{\sum_{j=1}^d \mathbf{I}[j]}.$$

A lower entropy indicates more focused attribution on a few features, while a higher value suggests more uniform reliance across all descriptors.

Together, these metrics evaluate the interpretability of GNNs from both structural (node-level) and semantic (feature-level) perspectives.

References

- [1] T. N. Kipf, M. Welling, Semi-supervised classification with graph convolutional networks, in: International Conference on Learning Representations, 2017, p. none.
URL <https://openreview.net/forum?id=SJU4ayYgI>
- [2] W. L. Hamilton, R. Ying, J. Leskovec, Inductive representation learning on large graphs, in: Proc. Adv. Neural Inf. Process. Syst., Vol. 30, 2017, pp. 1025–1035, <https://dl.acm.org/doi/pdf/10.5555/3294771.3294869>.
- [3] K. Xu, W. Hu, J. Leskovec, S. Jegelka, How powerful are graph neural networks?, in: Proc. Adv. Neural Inf. Process. Syst., Vol. 32, 2019, pp. 6201–6210, <https://openreview.net/forum?id=ryGs6iA5Krn>.
- [4] J. Gilmer, S. S. Schoenholz, P. F. Riley, O. Vinyals, G. E. Dahl, Neural message passing for quantum chemistry, in: International conference on machine learning, PMLR, 2017, pp. 1263–1272, <https://dl.acm.org/doi/pdf/10.5555/3305381.3305512>.
- [5] V. Gligorijević, P. D. Renfrew, T. Kosciolk, J. K. Leman, D. Berenberg, T. Vatanen, C. Chandler, B. C. Taylor, I. M. Fisk, H. Vlamakis, et al., Structure-based protein function prediction using graph convolutional networks, Nature communications 12 (1) (2021) 3168, <https://www.nature.com/articles/s41467-021-23303-9>.
- [6] Z. Guo, H. Wang, A deep graph neural network-based mechanism for social recommendations, IEEE Transactions on Industrial Informatics 17 (4) (2020) 2776–2783, <https://ieeexplore.ieee.org/document/9063418>.
- [7] Z. Wu, S. Pan, F. Chen, G. Long, C. Zhang, S. Y. Philip, A comprehensive survey on graph neural networks, IEEE transactions on neural networks and learning systems 32 (1) (2020) 4–24, <https://ieeexplore.ieee.org/document/9831453>.
- [8] P. Veličković, G. Cucurull, A. Casanova, A. Romero, P. Liò, Y. Bengio, Graph attention networks, in: International Conference on Learning Representations, 2018, p. none.
URL <https://openreview.net/forum?id=rJXMpikCZ>
- [9] S. Brody, U. Alon, E. Yahav, How attentive are graph attention networks?, in: International Conference on Learning Representations, 2022, p. none.
URL <https://openreview.net/forum?id=F72ximsx7C1>
- [10] J. Zhang, X. Shi, J. Xie, H. Ma, I. King, D. Y. Yeung, Gaan: Gated attention networks for learning on large and spatiotemporal graphs, in: Conference on Uncertainty in Artificial Intelligence, 2018, p. none.
URL <https://api.semanticscholar.org/CorpusID:3973810>
- [11] Y. Rong, W. Huang, T. Xu, J. Huang, Dropedge: Towards deep graph convolutional networks on node classification, in: International Conference on Learning Representations, 2020, p. none.
URL <https://openreview.net/forum?id=Hkx1qkrKPr>
- [12] C. Ying, T. Cai, S. Luo, S. Zheng, G. Ke, D. He, Y. Shen, T.-Y. Liu, Do transformers really perform badly for graph representation?, Advances in neural information processing systems 34 (2021) 28877–28888, <https://openreview.net/forum?id=OeWooXfWda>.
- [13] P. Jain, Z. Wu, M. A. Wright, A. Mirhoseini, J. E. Gonzalez, I. Stoica, Representing long-range context for graph neural networks with global attention, in: A. Beygelzimer, Y. Dauphin, P. Liang, J. W. Vaughan (Eds.), Advances in Neural Information Processing Systems, 2021, p. none.
URL https://openreview.net/forum?id=nYz2_BbZnYk
- [14] M. Brockschmidt, Gnn-film: Graph neural networks with feature-wise linear modulation, in: International Conference on Machine Learning, PMLR, 2020, pp. 1144–1152, <https://openreview.net/forum?id=HJe4Cp4KwH>.
- [15] L. Rampáček, M. Galkin, V. P. Dwivedi, A. T. Luu, G. Wolf, D. Beaini, Recipe for a general, powerful, scalable graph transformer, Advances in Neural Information Processing Systems 35 (2022) 14501–14515, <https://openreview.net/pdf?id=IMMaNf6oxKM>.

- [16] D. Bo, C. Shi, L. Wang, R. Liao, Specformer: Spectral graph neural networks meet transformers, in: ICLR, OpenReview.net, 2023, p. none, <https://openreview.net/pdf?id=0pdSt3oyJa1>.
- [17] D. Beaini, S. Passaro, V. Létourneau, W. Hamilton, G. Corso, P. Liò, Directional graph networks, in: International Conference on Machine Learning, PMLR, 2021, pp. 748–758, <https://openreview.net/forum?id=FUdBF49WRV1>.
- [18] J. Kim, D. Nguyen, S. Min, S. Cho, M. Lee, H. Lee, S. Hong, Pure transformers are powerful graph learners, *Advances in Neural Information Processing Systems* 35 (2022) 14582–14595.
- [19] J. Zhang, H. Zhang, C. Xia, L. Sun, Graph-bert: Only attention is needed for learning graph representations, *arXiv preprint arXiv:2001.05140* (2020).
- [20] M. Aqil, S. Atasoy, M. L. Kringelbach, R. Hindriks, Graph neural fields: A framework for spatiotemporal dynamical models on the human connectome, *PLoS Computational Biology* 17 (1) (2021) e1008310.
- [21] L. Jing, R. Dangovski, M. Soljacic, Waveletnet: Logarithmic scale efficient convolutional neural networks for edge devices, *arXiv preprint arXiv:1811.11644* (2018).
- [22] S. S. Du, K. Hou, R. R. Salakhutdinov, B. Póczos, R. Wang, K. Xu, Graph neural tangent kernel: Fusing graph neural networks with graph kernels, *Advances in neural information processing systems* 32 (2019).
- [23] N. M. Kriege, F. D. Johansson, C. Morris, A survey on graph kernels, *Applied Network Science* 5 (2020) 1–42.
- [24] A. Rahimi, B. Recht, Random features for large-scale kernel machines, *Advances in neural information processing systems* 20 (2007).
- [25] A. Vaswani, N. Shazeer, N. Parmar, J. Uszkoreit, L. Jones, A. N. Gomez, Ł. Kaiser, I. Polosukhin, Attention is all you need, *Advances in neural information processing systems* 30 (2017).
- [26] A. R. Barron, Universal approximation bounds for superpositions of a sigmoidal function, *IEEE Transactions on Information Theory* 39 (3) (1993) 930–945.
- [27] J. Atwood, D. Towsley, Diffusion-convolutional neural networks, *Advances in neural information processing systems* 29 (2016).
- [28] M. Zhang, Z. Cui, M. Neumann, Y. Chen, An end-to-end deep learning architecture for graph classification, in: Proceedings of the Thirty-Second AAAI Conference on Artificial Intelligence and Thirtieth Innovative Applications of Artificial Intelligence Conference and Eighth AAAI Symposium on Educational Advances in Artificial Intelligence, AAAI’18/IAAI’18/EAAI’18, AAAI Press, 2018, p. 8.
- [29] H. Maron, H. Ben-Hamu, N. Shafir, Y. Lipman, Invariant and equivariant graph networks, *arXiv preprint arXiv:1812.09902* (2018).
- [30] H. Maron, H. Ben-Hamu, H. Serviansky, Y. Lipman, Provably powerful graph networks, *Advances in neural information processing systems* 32 (2019).
- [31] P. de Haan, T. S. Cohen, M. Welling, Natural graph networks, *Advances in neural information processing systems* 33 (2020) 3636–3646.
- [32] G. Bouritsas, F. Frasca, S. Zafeiriou, M. M. Bronstein, Improving graph neural network expressivity via subgraph isomorphism counting, *IEEE Transactions on Pattern Analysis and Machine Intelligence* 45 (1) (2022) 657–668.
- [33] C. Bodnar, F. Frasca, Y. Wang, N. Otter, G. F. Montufar, P. Lio, M. Bronstein, Weisfeiler and lehman go topological: Message passing simplicial networks, in: International Conference on Machine Learning, PMLR, 2021, pp. 1026–1037.
- [34] C. Bodnar, F. Frasca, N. Otter, Y. Wang, P. Lio, G. F. Montufar, M. Bronstein, Weisfeiler and lehman go cellular: Cw networks, *Advances in neural information processing systems* 34 (2021) 2625–2640.
- [35] Q. Truong, P. Chin, Weisfeiler and lehman go paths: Learning topological features via path complexes, in: Proceedings of the AAAI Conference on Artificial Intelligence, Vol. 38, 2024, pp. 15382–15391.
- [36] J. Sun, C. Yang, X. Ji, Q. Huang, S. Wang, Towards dynamic message passing on graphs, *arXiv preprint arXiv:2410.23686* (2024).
- [37] J. Baek, M. Kang, S. J. Hwang, Accurate learning of graph representations with graph multiset pooling, *arXiv preprint arXiv:2102.11533* (2021).
- [38] J. Wu, X. Chen, K. Xu, S. Li, Structural entropy guided graph hierarchical pooling, in: International conference on machine learning, PMLR, 2022, pp. 24017–24030.
- [39] Y. Chen, Y. R. Gel, Topological pooling on graphs, in: Proceedings of the AAAI Conference on Artificial Intelligence, Vol. 37, 2023, pp. 7096–7103.
- [40] C. Liu, W. Yu, K. Gao, X. Ma, Y. Zhan, J. Wu, W. Hu, B. Du, Graph explicit pooling for graph-level representation learning, *Neural Networks* 181 (2025) 106790.
- [41] Y. Zhang, L. Li, K. Xia, Rhomboid tiling for geometric graph deep learning (2025). *arXiv:2505.09586*. URL <https://arxiv.org/abs/2505.09586>
- [42] E. Chien, J. Peng, P. Li, O. Milenkovic, Adaptive universal generalized pagerank graph neural network, *arXiv preprint arXiv:2006.07988* (2020).
- [43] J. Gasteiger, A. Bojchevski, S. Günnemann, Predict then propagate: Graph neural networks meet personalized pagerank, *arXiv preprint arXiv:1810.05997* (2018).
- [44] Y. Shi, Z. Huang, S. Feng, H. Zhong, W. Wang, Y. Sun, Masked label prediction: Unified message passing model for semi-supervised classification, *arXiv preprint arXiv:2009.03509* (2020).
- [45] D. Kreuzer, D. Beaini, W. Hamilton, V. Létourneau, P. Tossou, Rethinking graph transformers with spectral attention, *Advances in Neural Information Processing Systems* 34 (2021) 21618–21629.
- [46] J. Chen, K. Gao, G. Li, K. He, Nagphormer: A tokenized graph transformer for node classification in large graphs, *arXiv preprint arXiv:2206.04910* (2022).
- [47] H. Shirzad, A. Vellingker, B. Venkatchalam, D. J. Sutherland, A. K. Sinop, Exphormer: Sparse transformers for graphs, in: International Conference on Machine Learning, PMLR, 2023, pp. 31613–31632.
- [48] L. Van der Maaten, G. Hinton, Visualizing data using t-sne., *Journal of machine learning research* 9 (11) (2008).
- [49] Z. Ying, D. Bourgeois, J. You, M. Zitnik, J. Leskovec, Gnnexplainer: Generating explanations for graph neural networks, *Advances in neural information processing systems* 32 (2019).
- [50] M. Dhaini, K. Z. Hussain, E. Zaradoukas, G. Kasneci, Evalxnp: A framework for benchmarking post-hoc explainability methods on nlp models, *arXiv preprint arXiv:2505.01238* (2025).
- [51] P. Chalasani, J. Chen, A. R. Chowdhury, X. Wu, S. Jha, Concise explanations of neural networks using adversarial training, in: H. D. III, A. Singh (Eds.), Proceedings of the 37th International Conference on Machine Learning, Vol. 119 of Proceedings of Machine Learning Research, PMLR, 2020, pp. 1383–1391. URL <https://proceedings.mlr.press/v119/chalasani20a.html>
- [52] Y. Zhang, D. Defazio, A. Ramesh, Relex: A model-agnostic relational model explainer, in: Proceedings of the 2021 AAAI/ACM Conference on AI, Ethics, and Society, AIES ’21, Association for Computing Machinery, New York, NY, USA, 2021, p. 1042–1049. doi:10.1145/3461702.3462562. URL <https://doi.org/10.1145/3461702.3462562>